Available online at www.sciencedirect.com
ScienceDirect
Trans. Nonferrous Met. Soc. China 29(2019) 2514−2522
Transactions of Nonferrous Metals Society of China
www.tnmsc.cn

Effect of ultrasonic assisted friction stir welding on microstructure and mechanical properties of AZ91−C magnesium alloy

Faraz BARADARANI, Amir MOSTAFAPOUR, Maghsoud SHALVANDI

Faculty of Mechanical Engineering, University of Tabriz, Tabriz, Iran

Received 18 March 2019; accepted 14 October 2019

Abstract: The influence of ultrasonic vibrations on microstructure and mechanical properties of the AZ91−C magnesium alloy after ultrasonic assisted friction stir welding (UaFSW) in comparison with conventional friction stir welding (FSW) was investigated. The FSW was applied at the rotational speed of 1400 r/min and welding speed of 40 mm/min and no defects were observed. Using the same welding parameters, the process was carried out with inducing ultrasonic vibrations to the weld line at the amplitude of 15 μm. The microstructure of the specimens was observed with optical and scanning electron microscopy. The results indicate that a very fine microstructure is obtained in UaFSW with respect to that of conventional FSW. Moreover, β-$Mg_{17}Al_{12}$ coarse dendrites are segregated to very fine and partly spherical particles that homogeneously distribute in α-Mg matrix. This remarkably-modified morphology of microstructure attributed to severe plastic deformation comes from ultrasonic vibration and friction stirring effect. Tensile and hardness tests were performed to evaluate the mechanical properties of the welds. According to the results, the vibration greatly improves the mechanical properties of the conventional FSW joint. The tensile strength and hardness are increased from 195 MPa and HV 79 in conventional FSW to 225 MPa and HV 87 in UaFSW, respectively.

Key words: ultrasonic assisted friction stir welding; AZ91 magnesium alloy; microstructure; mechanical properties

1 Introduction

Magnesium is the lightest metal used for constructions. Due to its excellent specific strength and stiffness, dimensional stability and high damping capacity, magnesium has been widely used in transportation and aerospace industries [1−3]. However, it exhibits low corrosion resistance and cold workability at room temperature due to its hexagonal closed-pack (HCP) crystal structure [4]. In order to overcome these limitations, magnesium must be alloyed with other metals for engineering applications [5,6]. Among the various magnesium alloys developed, AZ91 magnesium alloy is the most widely used [7]. CHEN et al [8] studied effects of pressurized solidification and microstructure modification on mechanical properties of AZ91 magnesium alloy. NIE et al [9] investigated the effect of multidirectional forging on microstructure and mechanical properties of AZ91 magnesium alloy. They concluded that the both tensile strength and elongation to failure were increased. Improved mechanical properties of AZ91 magnesium alloy through extrusion were presented by KIM et al [10]. Microstructure and morphology of precipitates in magnesium alloys with various severe plastic deformation methods have been studied in previous reports [11−17].

However, relatively little attention has been paid to the welding processes of AZ91 magnesium alloy, and a reliable welding process is essential for commercial application of AZ91 alloy. Conventional fusion welding processes such as plasma arc welding, tungsten inert gas or laser beam welding obstruct the application of magnesium alloys due to hot cracking, porosity, oxidation and high residual stress [18]. Friciton stir welding (FSW) is a green solid state welding process which can eliminate relevant fusion welding defects [19]. This technique can improve the mechanical properties of the material [20,21]. After FSW, different corrosion behaviors [22] and machining characteristics [23] of the material were observed. MOTALLEB-NEJAD et al [24] studied the effect of pin profile on microstructure and mechanical properties of AZ31 magnesium alloy. Friction stir spot welding (FSSW) of rare-earth ZEK 100 magnesium alloy sheets was investigated by RAO et al [25]. MIRONOV et al [26] investigated grain

Corresponding author: Amir MOSTAFAPOUR; Tel: +98-4133393822; Fax: +98-4133354153; E-mail: a-mostafapur@tabrizu.ac.ir
DOI: 10.1016/S1003-6326(19)65159-9

refinement during friction stir welding of AZ31 magnesium alloy. Effect of welding environment on microstructure of AZ91 Magnesium alloy was studied by ROUHI et al [27]. It is remarkable that eliminating all welding defects is not possible. There are relevant defects associated with FSW including lack of penetration, tunnel defect, worm hole, kissing bound and lazy S [28]. Improper welding parameters or inadequate temperature resulted in defects on the welds. Therefore, researchers mainly have focused on methods to diminish the welding defects and increase the mechanical properties of the welds [29]. To overcome these limitations, several hybrid FSW methods have been applied. These methods include the application of laser beam, inductive coil or electrical resistance as secondary energy source. It is remarkable that using secondary energy source leads to other undesirable problems and reduces inherent advantages of FSW [30]. Ultrasonic vibration improved the material flow in the welding, reduced the downward material flow stress without notable increase in peak temperature and produced high quality welds [31]. GAO et al [32] studied the effect of ultrasonic vibration on material flow and mechanical properties of AA 2024-T3 and concluded that ultrasonic vibration improved the material flow and increased the ductility of weld joints. WU et al [33] investigated the influence of ultrasonic vibration on fatigue performance of friction stir welded AA 2024-T3 and reported better fatigue life on ultrasonic assisted friction stir welding (UaFSW) specimens. Applying ultrasonic vibration in FSW is quite recent and only limited number of studies on UaFSW are recently published. These studies are mainly focused on aluminum alloys material flow and force analysis during UaFSW and inadequate attention was paid to microstructure of UaFSW on magnesium alloys. Recently, the microstructure and mechanical properties of ultrasonic enhanced FSW of Al 6061-T4 to Mg AZ31B were investigated by LV et al [34]. Their studies revealed that by inducing ultrasonic vibrations to the weld line, the mechanical interlocking and tensile properties of the weld were improved. The intermetallic compound layer completely fragmented and dispersed in α-Mg matrix, which results in improvement of the morphology of the welds [35]. The present work primarily is focused on microstructure, precipitates morphology and mechanical properties of UaFSWed AZ91 magnesium alloy in comparison with the conventional FSW.

2 Experimental

2.1 Materials and method

In the present investigation, AZ91−C magnesium alloy is applied as base metal (BM). The chemical composition of the BM is given in Table 1. Ultrasonic assisted friction stir welding and conventional friction stir welding were carried out on AZ91−C magnesium alloy. Plates with dimensions of 6 mm in thickness, 150 mm in length and 50 mm in width were subjected to the welding process in a bead-on-plate configuration [36].

Table 1 Chemical composition of BM AZ91−C magnesium alloy (wt. %)

Mg	Al	Zn	Mn	Cr	Fe	Si	Ni	Cu
90.80	8.20	0.68	0.16	0.10	0.04	0.01	0.003	0.001

A heat-treated non-consumable tool made of H13 tool steel was applied to UaFSW and FSW operations. Due to excellent combination of toughness and fatigue resistance, H13 is widely used in FSW applications [27,36−38]. Shoulder diameter of the tool is 18 mm and pin profile is square [32]. The photograph of welding tool and its geometry are shown in Fig. 1. UaFSW and FSW were carried out on a vertical milling machine. Welding process was performed for different process parameters based on the literature and also was precisely chosen to obtain successful performance of the process. Rotational speed was selected between 900 and 1800 r/min and traverse speed was 20−80 mm/min. The tilt angle was kept constant at 2.5° [36,39,40].

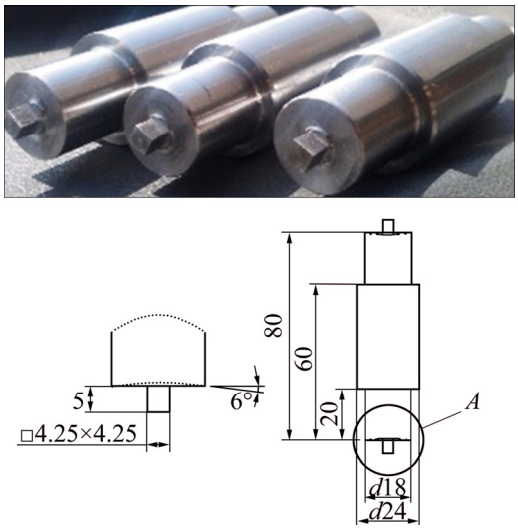

Fig. 1 Photograph of welding tool and its geometry (Unit: mm)

2.2 Ultrasonic setup preparation

Special fixture should be designed to hold the welding specimens together with ultrasonic setup in UaFSW. Due to the aim of investigating the effect of ultrasonic vibration in UaFSW, the vibration should be applied in the weld line. To restrict vibration damping effect of the fixture, the contact between specimen and fixture should be minimal. Figure 2 illustrates the designed and fabricated fixture with considering

above-mentioned points. As shown in Fig. 2(a), the ultrasonic horn and transducer were fixed together and the vibration was imposed normal to the weld line. The clamping fasteners, welding line and vibrating direction are illustrated in Fig. 2(b). The welding plate is tightly fastened to the fixture body only from two sides. Due to reasonable distance between the fasteners and welding area, the welding line can easily vibrate. The vibration amplitude of the specimens along the weld line was experimentally measured. Due to the large diameter of the horn, no significant damping effect was observed and the vibration amplitude in the weld line was almost constant. The similar welding setup was applied in previous works [41,42].

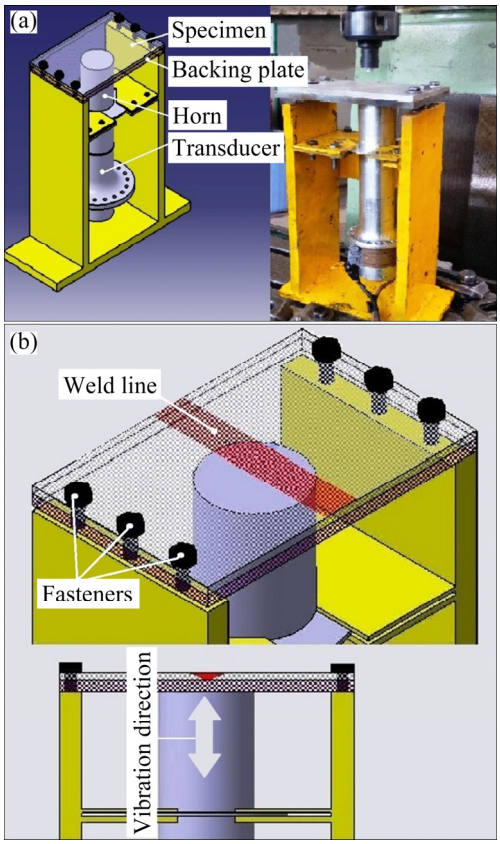

Fig. 2 Ultrasonic assisted and conventional FSW setup: (a) Vibration system component and fixture; (b) Clamping system and vibration direction

The ultrasonic setup consists of transmitting horn, transducer and generator. A 2000 W piezoelectric transducer was applied to generating ultrasonic vibration in specimens. Power supply covered 50−60 Hz with fixed input voltage of 220 V. The variable output voltage up to 500 V was used to adjust high frequency electrical pulse power. These pulses stimulated the transducer to produce mechanical vibration with the same frequency. The peak-to-peak amplitude of the vibration was 15 μm.

The ultrasonic horn was designed considering the transducer longitudinal resonance frequency. Due to high strength and ease of manufacturing, a cylindrical shape was designed. The dimensions of the horn were selected such a way that it could have resonance near 20 kHz. Modal analysis was performed by means of ANSYS 14.0 software. In the modal analysis, totally 3327 nodes and 1722 elements were used and the suitable horn length was obtained to be 131 mm. The natural resonance frequency of horn was equal to19795 Hz. Figure 3 illustrates the longitudinal mode shape of horn natural resonance frequency.

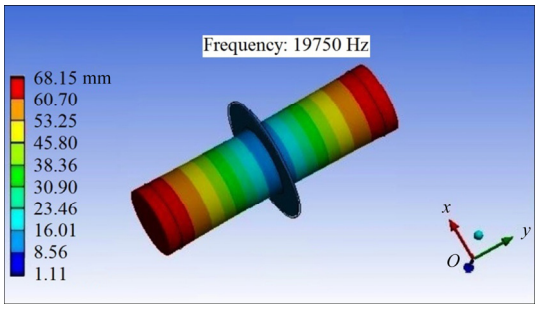

Fig. 3 Longitudinal mode shape of horn natural resonance frequency

2.3 Microstructure and mechanical properties analyses

The specimens were cut normal to welding direction and mechanically ground with Sic abrasive paper. Polishing of the specimens was performed on 20 N and 120 r/min using 3 μm diamond paste for 3 min and 0.5 μm diamond paste until a mirror-like surface was obtained. Specimens were etched with the acid mixture including 60 mL ethylene glycol, 20 mL citric acid, 1 mL HNO_3 and 20 mL distilled water [39]. The optical microscope (OM), OLYMPUS-BX57M, was used to capture the microscopic images of specimens and the grain size was determined by microstructural image processing (MIP). The scanning electron microscope (SEM), Ziess sigma HD, was used to study the microstructure and precipitates morphology of the weld. Tensile test was implemented based on ASTM: EM08 at constant strain rate of 1×10^{-5} s^{-1} and to obtain high accuracy results the test was repeated three times for each welding method. Specimens were cut with wire cut electro discharge machine in the direction of friction stir welding line. Vickers hardness test was performed on Reicherter UH250 hardness testing machine. The hardness test positions were chosen in the center of the weld. The specimens were cut across the weld line and hardness measurements in 10 s under 980 N load were carried out on 4 regions including BM, heat-affected zone (HAZ), thermomechanically-affected zone (TMAZ) and stir zone (SZ) [43].

3 Results and discussion

3.1 Welding parameters

The photographs of bead-on-plate weld with different process parameters are presented in Fig. 4 and post weld observations are summarized in Table 2. The results show the crucial role of rotational speed and traverse speed on successful welding. By increasing the rotational speed to the limit of 1600 r/min, the generated heat is increased and excessive material flush is noticed along the weld. When the tool traverse speed is greater than 40 mm/min, the poor material flow causes groove and cracks in the weld line. Successful and sound welds are obtained at 1400 r/min rotational speed and 40 mm/min traverse speed. So, UaFSW and conventional FSW were performed on specimens at 1400 r/min rotational speed and 40 mm/min traverse speed. The welding fixture is the same for both processes and the only difference is ultrasonic vibration.

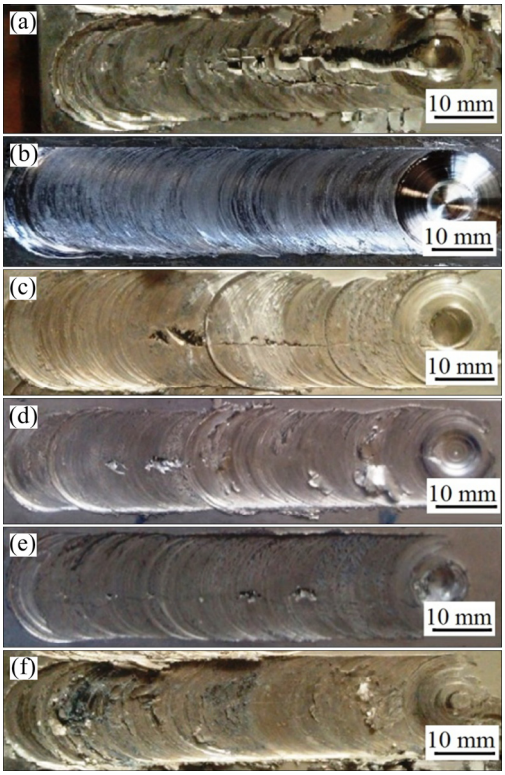

Fig. 4 Photographs of weld obtained at different tool rotational speeds and traverse speeds: (a) 900 r/min and 80 mm/min; (b) 1200 r/min and 80 mm/min; (c) 1200 r/min and 40 mm/min; (d) 1400 r/min and 40 mm/min; (e) 1400 r/min and 60 mm/min; (f) 1600 r/min and 20 mm/min

3.2 Microstructure characterization

Figure 5 illustrates the optical micrographs of the BM and different welding areas of AZ91 magnesium alloy obtained at 1400 r/min and 40 mm/min. As shown in Fig. 5(a) and Fig. 5(b), the BM has coarse grain α-Mg matrix surrounded with β-$Mg_{17}Al_{12}$ dendrite or β+α phases. Similar microstructure for as-cast magnesium AZ91 alloy was reported in other works [43−45]. The backscattered scanning electron (BSE) micrographs (Figs. 6(a, b)) of base metal confirm the optical micrographs results. The EDX point analysis results of Fig. 6 are summarized in Table 3. The dark areas in the BM are mainly α-Mg grains and the amount of Al is determined to be (3.3±0.1) wt.% which is higher than the equilibrium maximum solid solubility of Al (1.5 wt.%) in Mg at room temperature [46]. It has been shown that Al slightly supersaturates in α-Mg. The gray dendritic areas are determined as β-$Mg_{17}Al_{12}$ which include Zn solute atoms. It has been reported that in Mg−Al−Zn alloys, Zn mainly substitutes Al and forms a new intermetalic $Mg_{17}Zn_{12}$ phase [47,48]. For FSW and UaFSW specimens, α-Mg matrix presents an increase in Al content. The average content of Al in FSW and UaFSW is obtained by sampling four testing point which is equal to 6.4 and 7.7 wt.%, respectively, which is much higher than the Al content for BM. Therefore, it is inferred that the particles of β-phase have been resolved again in α-Mg during FSW and UaFSW.

Table 2 Weld joint status at different process parameters

No.	Rotational speed/(r·min^{-1})	Traverse speed/(mm·min^{-1})	Observation
1	900	80	Insufficient heat, wide groove
2	1200	80	Insufficient heat, linear crack
3	1200	40	Insufficient heat, narrow crack
4	1400	40	Sound weld
5	1400	60	Excessive flush, crack
6	1600	20	Excessive heat and flush, poor weld

The optical micrographs of welded specimens are presented in Figs. 5(c, d). Three characteristics of FSW areas are distinguishable in both welding methods. The grains are refined and dynamic recrystallization (DRX) takes place in stir zone of FSW and UaFSW. As shown in Figs. 5(e, f), the stir zone in both methods has smaller grain size in comparison with BM but UaFSW specimen has finer grain structure in comparison with FSW specimen. The average grain size of BM is 80 μm, that of SZ of FSW is 4 μm and that of SZ of UaFSW is 1.8 μm. The reason behind this could be the dynamic recrystallization in the stir zone [49]. During the welding process, the material in the weld region is subjected to

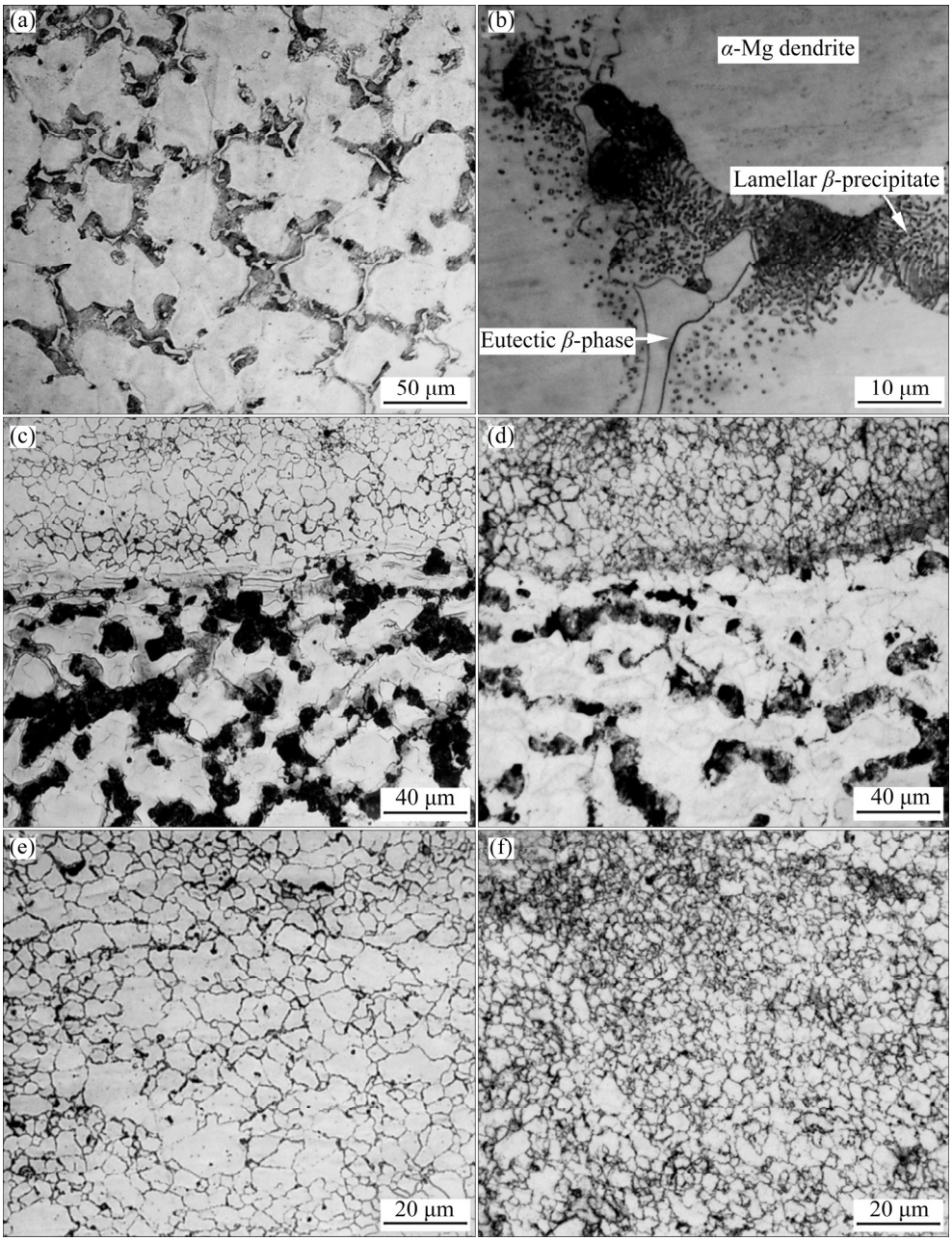

Fig. 5 Optical micrographs of different AZ91 samples: (a) Base metal; (b) High magnification of BM precipitates; (c) FSWed sample; (d) UaFSWed sample; (e) Stir zone of FSW; (f) Stir zone of UaFSW

severe plastic deformation and density of dislocations in the stir zone increases significantly. Due to the high temperature, dislocations in the structure create low angle grain boundaries (LAGB) for the purpose of reducing the free energy of the material. By increasing the amounts of deformation, the sub-grains are converted into high angle grain boundaries (HAGB), and as a result, new grains form within the initial grains and fine grain structure is obtained [49]. During the UaFSW, due to the vibration of weld, the material in the SZ has higher strain than the material in the SZ of conventional FSW. There is a direct relation between the strain and the dislocation density of the strained material [49]. Hence, the density of dislocation in the stir zone of the UaFSW is greater than the density of dislocation in the conventional FSW, and therefore, during the dynamic recrystallization in UaFSW, more HAGBs form and the weld zone with finer grain size is obtained.

UaFSW specimens illustrate homogenous ultrafine-grained microstructure without apparent dendrite β phase. Highly magnified BSE images of α-Mg phase for conventional FSW and UaFSW are presented in Figs. 6(c) and 6(d), respectively. The β-phase fragments into fine particles that homogenously distribute in α-Mg matrix. Better distribution and finer particle are obtained with UaFSW. This remarkably modified morphology of

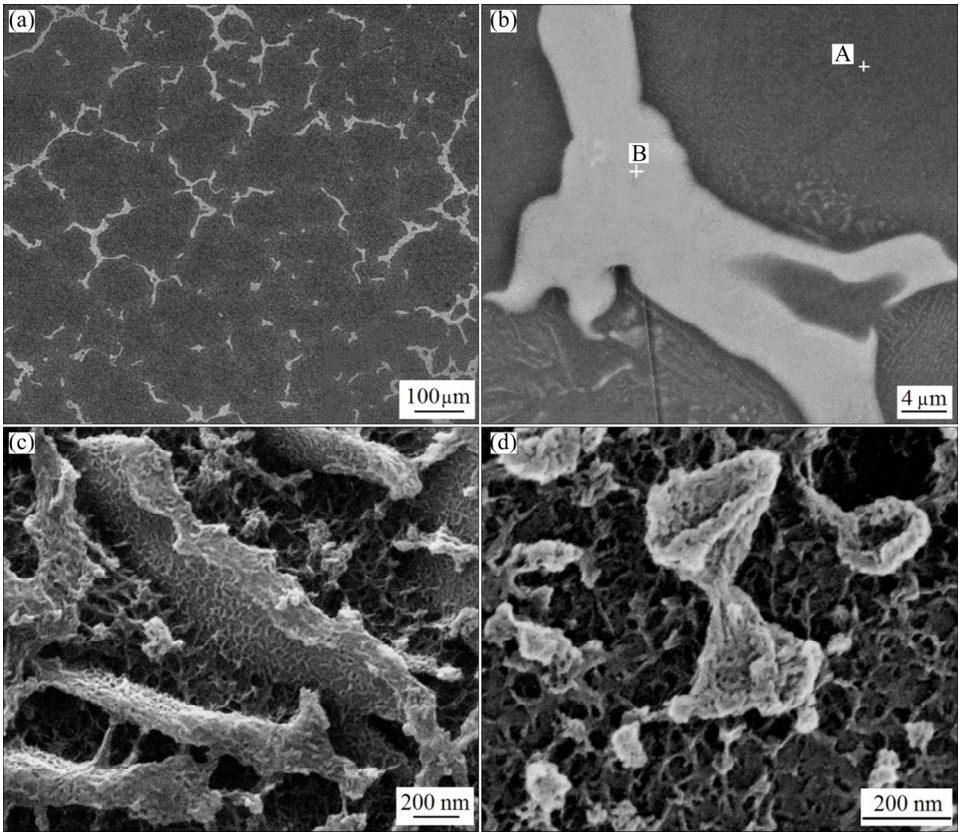

Fig. 6 BSE micrographs of different AZ91 samples: (a) Base metal; (b) High magnification of BM precipitates; (c) Precipitates in SZ of FSWed sample; (d) Precipitates in SZ of UaFSWed sample

Table 3 Chemical compositions of BM, FSW and UaFSW specimens (wt.%)

Point	Mg	Al	Zn
A (α-Mg)	96.7±0.9	3.3±0.1	–
B (β-$Mg_{17}Al_{12}$)	63±0.4	31.3±0.5	5.7±0.4
SZ of FSW	92.9±0.3	6.4±0.6	0.7±0.1
SZ of UaFSW	91.5±0.3	7.7±0.5	0.8±0.1

microstructure attributed to severe plastic deformation comes from ultrasonic vibration and friction stirring effect.

3.3 Mechanical properties

Figure 7 illustrates the comparison of Vickers hardness profiles for UaFSW and FSW. As shown in Fig. 7, there is the same manner for hardness diagrams in both welds. Due to the severe plastic deformation and dynamic recrystallization, the hardness of SZ is higher than that of other areas. The friction stir welding enhanced with ultrasonic vibration yields higher value of hardness compared to the conventional friction stir welding. The reason could be the finer grain structure, better distribution of β-phase, and hardening effect of intense stirring action in the welding area and mechanical work originated from ultrasonic vibration.

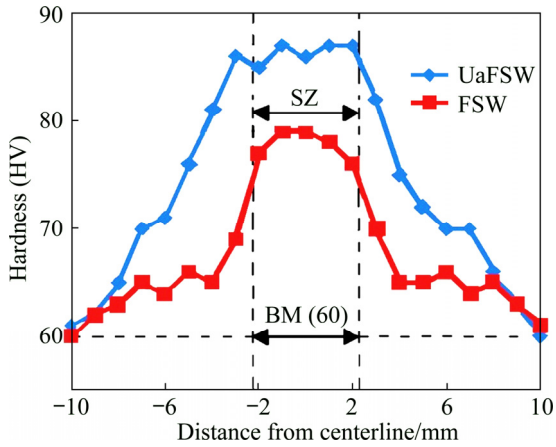

Fig. 7 Hardness profiles of UaFSW and FSW joints

Figure 8 shows the yield strength (YS), ultimate tensile strength (UTS) and elongation (ELG) for BM, conventional FSW and UaFSW. The YS values of BM, FSW and UaFSW are 75, 115 and 130 MPa, respectively. Due to similar strengthening effect, the YS values for specimens correspond well with their average hardness values. The BM exhibits the lowest UTS of 125 MPa and ELG of 2%. After FSW, the UTS and ELG are increased to 195 MPa and 4%, respectively. It is shown that UaFSW specimens exhibit UTS of 225 MPa and ELG of 5% which is much higher than the values of BM. After

UaFSW, the average size of the grains decreases to 1.8 μm and eutectic network and rough precipitates segregate to ultra-fine and homogenously-distributed particles. The large number of β-phase particles increases the strength of the material and their sub micron size diminishes cavitations and micro-cracks at the interface between α-Mg and β-phase [50]. The fine-grain structure and homogenously-distributed particles result in stress dispersion and delay stress concentration to a large extend. By reducing grain size, the volumetric component of the grain boundaries increases. Since the grain boundaries act as barriers to the motion of dislocations, the strength increases. In such a fine-grain structure, non-basal slip planes can be activated in favor of harmonized deformation and consequently the ductility is improved [51]. The fine-grain structure and dispersed particles significantly increase the strength and toughness of the material. By using ultrasonic vibration on FSW, notable improvements in tensile properties are obtained.

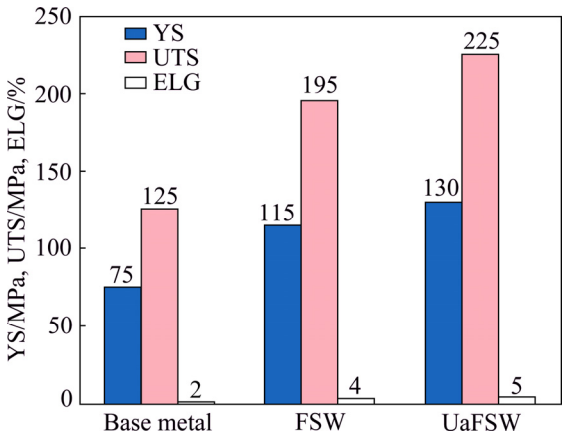

Fig. 8 Comparison of yield stress (YS), ultimate strength (UTS) and elongation (ELG) for BM, FSW and UaFSW joints

4 Conclusions

(1) AZ91−C magnesium alloy was successfully welded by UaFSW and no defects were found by applying tool rotational speed of 1400 r/min and traverse speed of 40 mm/min.

(2) FSW can refine the grains of AZ91 Mg alloy from 80 to 4 μm in the stir zone, but further refinement is obtained via UaFSW with average grain size of 1.8 μm.

(3) In FSW, dendrite β-phases are segregated to fine particles homogenously distributing in α-Mg, and finer particles and better morphology are obtained by UaFSW.

(4) In comparison with BM, significant improvements in the tensile properties are achieved in the FSW due to fine grain structure and better β-phase distribution. The UaFSW leads to higher tensile strength, elongation and hardness values.

(5) Ultrasonic vibration plays an important role in microstructure evolution during UaFSW.

References

[1] MORDIKE B L, EBERT T. Magnesium: Properties−applications–potential [J]. Materials Science and Engineering A, 2001, 302: 37−45.

[2] BAMBERGER M, DEHM G. Trends in the development of new Mg alloys [J]. Annual Review of Materials Research, 2008, 38: 505−533.

[3] YANG Z, LI J P, ZHANG J X, LORIMER G W, ROBSON J. Review on research and development of magnesium alloys [J]. Acta Metallurgica Sinica (English letters), 2008, 21(5): 313−328.

[4] KAMAL JAYARAJ R, MALARVIZHI S, BALASUBRAMANIAN V. Electrochemical corrosion behaviour of stir zone of friction stir welded dissimilar joints of AA6061 aluminium–AZ31B magnesium alloys [J]. Transactions of Nonferrous Metals Society of China, 2017, 27(10): 2181−2192.

[5] COMMIN L, DUMONT M, MASSE J E, BARRALLIER L. Friction stir welding of AZ31 magnesium alloy rolled sheets influence of processing parameters [J]. Acta Materialia, 2009, 57(2): 326−334.

[6] MUNITZ A, COTLER C, STERN A, KOHN G. Mechanical properties and microstructure of gas tungsten arc welded magnesium AZ91D plates [J]. Materials Science and Engineering A, 2001, 302: 68−73.

[7] CZERWINSKI F. The oxidation behaviour of an AZ91D magnesium alloy at high temperatures [J]. Acta Materialia, 2002, 50(10): 2639−2654.

[8] CHEN S N, YANG W, YU H, ZHANG Y L. Effects of microstructure modification and pressurized solidification on mechanical property of AZ91 alloy [J]. Journal of Alloys and Compounds, 2014, 611: 1−6.

[9] NIE K B, DENG K K, WANG X J, XU F J, WU K, ZHENG M Y. Multidirectional forging of AZ91 magnesium alloy and its effects on microstructures and mechanical properties [J]. Materials Science and Engineering A, 2015, 624: 157−168.

[10] KIM Sang-hoon, LEE Jong-un, KIM Ye-jin, MOON Byoung-gi, YOU Bong-sun, KIM Ha-sik, PARK Sung-hyuk. Improvement in extrude ability and mechanical properties of AZ91 alloy through extrusion with artificial cooling [J]. Materials Science and Engineering A, 2017, 703: 1−8.

[11] MATHIS K, GUBICZA J, NAM N H. Microstructure and mechanical behavior of AZ91 Mg alloy processed by equal channel angular pressing [J]. Journal of Alloys and Compounds, 2005, 394: 194−199.

[12] GUO Wei, WANG Qu-dong, YE Bing, ZHOU Hao. Microstructure and mechanical properties of AZ31 magnesium alloy processed by cyclic closed-die forging [J]. Journal of Alloys and Compounds, 2013, 558: 164−171.

[13] RAVI KUMAR N V, BLANDIN J J, DESRAYAUD C, MONTHEILLET F, SUERY M. Grain refinement in AZ91 magnesium alloy during thermo mechanical processing [J]. Materials Science and Engineering A, 2003, 359: 150−157.

[14] MUSSI A, BLANDIN J J, SALVO L, RAUCH E F. Resistance to strain-induced damage of an ultrafine-grained magnesium alloy deformed in superplastic conditions [J]. Acta Materialia, 2006, 54(14): 3801−3809.

[15] KAI M, HORITA Z, LANGDON T G. Developing grain refinement and superplasticity in a magnesium alloy processed by high-pressure torsion [J]. Materials Science and Engineering A, 2008, 488: 117−124.

[16] XING Jie, SODA H, YANG Xu-yue, MIURA H, SAKAI T. Ultra-fine grain development in an AZ31 magnesium alloy during

multi-directional forging under decreasing temperature conditions [J]. Materials Transactions, 2005, 46: 1646−1650.

[17] BUSSIBA A, BEN ARTZY A, SHTECHMAN A, IFERGAN S, KUPIEC M. Grain refinement of AZ31 and ZK60 Mg alloys towards superplasticity studies [J]. Materials Science and Engineering A, 2001, 302: 56−62.

[18] PAN Fu-sheng, XU An-lian, DENG De-an, YE Jun-hua, JIANG Xian-quan, TANG Ai-tao, RAN Yang. Effects of friction stir welding on microstructure and mechanical properties of magnesium alloy Mg−5Al−3Sn [J]. Materials & Design, 2016, 110: 266−274.

[19] WAHID M A, KHAN Z A, SIDDIQUEE A N. Review on underwater friction stir welding: A variant of friction stir welding with great potential of improving joint properties [J]. Transactions of Nonferrous Metals Society of China, 2018, 28(2): 193−219.

[20] SHARMA C, UPADHYAY V, DWIVEDI D K, KUMAR P. Mechanical properties of friction stir welded armor grade Al−Zn−Mg alloy joints [J]. Transactions of Nonferrous Metals Society of China, 2017, 27(3): 493−506.

[21] SHANAVAS S, EDWIN RAJA DHAS J. Parametric optimization of friction stir welding parameters of marine grade aluminium alloy using response surface methodology [J]. Transactions of Nonferrous Metals Society of China, 2017, 27(11): 2334−2344.

[22] MENG Qiang, LIU Yang, KANG Ju, FU Rui-dong, GUO Xiao-yan, LI Yi-jun. Effect of precipitate evolution on corrosion behavior of friction stir welded joints of AA2060-T8 alloy [J]. Transactions of Nonferrous Metals Society of China, 2019, 29(4): 701−709.

[23] SURYA KIRAN G V V, HARI KRISHNA K, SAMEER S, BHARGAVI M, SANTOSH KUMAR B, MOHANA RAO G, NAIDUBABU Y, DUMPALA R, RATNA SUNIL B. Machining characteristic of fine grained AZ91 Mg alloy processed by friction stir processing [J]. Transactions of Nonferrous Metals Society of China, 2017, 27(4): 804−811.

[24] MOTALLEB-NEJAD P, SAEID T, HEYDARZADEH A, DARZI K H, ASHJARI M. Effect of tool pin profile on microstructure and mechanical properties of friction stir welded AZ31B magnesium alloy [J]. Materials & Design, 2014, 59: 221−226.

[25] RAO H M, RODRIGUEZ R I, JORDON J B, BARKEY M E, GUO Y B, BADARINARAYAN H, YUAN W. Friction stir spot welding of rare-earth containing ZEK100 magnesium alloy sheets [J]. Materials & Design, 2014, 56: 750−754.

[26] MIRONOV S, ONUMA T, SATO Y S, KOKAWA H. Microstructure evolution during friction-stir welding of AZ31 magnesium alloy [J]. Acta Materialia, 2015, 100: 301−312.

[27] ROUHI S, MOSTAFAPOUR A, ASHJARI M. Effects of welding environment on microstructure and mechanical properties of friction stir welded AZ91C magnesium alloy joints [J]. Science and Technology of Welding and Joining, 2016, 21(1): 25−31.

[28] CHEN Hua-bin, YAN Keng, LIN Tao, CHEN Shan-ben, JIANG Cheng-yu, ZHAO Yong. The investigation of typical welding defects for 5456 aluminum alloy friction stir welds [J]. Materials Science and Engineering A, 2006, 433: 64−69.

[29] KUMAR S. Ultrasonic assisted friction stir processing of 6063 aluminum alloy [J]. Archives of Civil and Mechanical Engineering, 2016, 16: 473−484.

[30] PADHY G K, WU C S, GAO S. Auxiliary energy assisted friction stir welding-status review [J]. Science and Technology of Welding and Joining, 2015, 20(8): 631−649.

[31] LIU Zhen-lei, MENG Xiang-chen, JI Shu-de, LI Zheng-wei, WANG Lin. Improving tensile properties of Al/Mg joint by smashing intermetallic compounds via ultrasonic-assisted stationary shoulder friction stir welding [J]. Journal of Manufacturing Processes, 2018, 31: 552−558.

[32] GAO S, WU C S, PADHY G K. Material flow, microstructure and mechanical properties of friction stir welded AA 2024-T3 enhanced by ultrasonic vibrations [J]. Journal of Manufacturing Processes, 2017, 30: 385−395.

[33] WU Ming-xiao, WU Chuan-song, GAO Song. Effect of ultrasonic vibration on fatigue performance of AA2024-T3 friction stir weld joints [J]. Journal of Manufacturing Processes, 2017, 29: 85−95.

[34] LV X Q, WU C S, PADHY G K. Diminishing intermetallic compound layer in ultrasonic vibration enhanced friction stir welding of aluminum alloy to magnesium alloy [J]. Materials Letters, 2017, 203: 81−84.

[35] LV Xue-qi, WU Chuan-song, YANG Chun-liang, PADHY G K. Weld microstructure and mechanical properties in ultrasonic enhanced friction stir welding of Al alloy to Mg alloy [J]. Journal of Materials Processing Technology, 2018, 254: 145−157.

[36] ROUHI S, DADASHPOUR M, MOSTAFAPOUR A, DONIAVI A. Effects of multi-pass FSP on the β phase ($Mg_{17}Al_{12}$) distribution and mechanical properties of AZ91C magnesium alloy [J]. Journal of Achievements in Materials and Manufacturing Engineering, 2017, 82(2): 77−85.

[37] LAKSHMANA PRASAD B, NEELAIAH G, GOPI KRISHNA M, RAMANA S V V, SAI PRAKASH K, SARIKA G, PRADEEP KUMAR REDDY G, DUMPALA R, RATNA SUNIL B. Joining of AZ91 Mg alloy and Al6063 alloy sheets by friction stir welding [J]. Journal of Magnesium and Alloys, 2018, 6(1): 71−76.

[38] SINGARAPU U, ADEPU K, ARUMALLE S R. Influence of tool material and rotational speed on mechanical properties of friction stir welded AZ31B magnesium alloy [J]. Journal of Magnesium and Alloys, 2015, 3(4): 335−344.

[39] TAN Shuai, ZHENG Fei-yan, CHEN Juan, HAN Jing-yu, WU Yu-juan, PENG Li-ming. Effects of process parameters on microstructure and mechanical properties of friction stir lap linear welded 6061 aluminum alloy to NZ30K magnesium alloys [J]. Journal of Magnesium and Alloys, 2017, 5(1): 56−63.

[40] KHAYYAMIN D, MOSTAFAPOUR A, KESHMIRI R. The effect of process parameters on microstructural characteristics of AZ91/SiO_2 composite fabricated by FSP [J]. Materials Science and Engineering A, 2013, 559: 217−221.

[41] LIU Zhen-lei, JI Shu-de, MENG Xiang-chen. Joining of magnesium and aluminum alloys via ultrasonic assisted friction stir welding at low temperature [J]. The International Journal of Advanced Manufacturing Technology, 2018, 97: 4127−4136.

[42] JI Shu-de, MENG Xiang-chen, LIU Zhen-lei, HUANG Ruo-fei, LI Zheng-wei. Dissimilar friction stir welding of 6061 aluminum alloy and AZ31 magnesium alloy assisted with ultrasonic [J]. Materials Letters, 2017, 201: 173−176.

[43] UGENDER D S. Influence of tool pin profile and rotational speed on the formation of friction stir welding zone in AZ31 magnesium alloy [J]. Journal of Magnesium and Alloys, 2018, 6(2): 205−213.

[44] ZHAO Ming-chun, LIU Ming, SONG Guang-ling, ATRENS A. Influence of the β-phase morphology on the corrosion of the Mg alloy AZ91 [J]. Corrosion Science, 2008, 50(7): 1939−1953.

[45] SINGH RAMAN R K, BIRBILIS N, EFTHIMIADIS J. Corrosion of Mg alloy AZ91−The role of microstructure [J]. Corrosion Engineering Science and Technology, 2004, 39(4): 346−350.

[46] CELOTTO S, BASTOW T J. Study of precipitation in aged binary Mg−Al and ternary Mg−Al−Zn alloy using 27 Al NMR spectroscopy [J]. Acta Materialia, 2001, 49(1): 41−51.

[47] CHAI Fang, ZHANG Da-tong, LI Yuan-yuan. Microstructures and tensile properties of submerged friction stir processed AZ91 magnesium alloy [J]. Journal of Magnesium and Alloys, 2015, 3(3): 203−209.

[48] ESMAILY M, MORTAZAVI N, SVENSSON J E, HALVARSSON M, BIUCHER D B, JARFORS A E W, WESSEN M, JOHNSSON L G. Atmospheric corrosion of Mg alloy AZ91 fabricated by a

semi-solid casting technique: The influence of microstructure [J]. Journal of the Electrochemical Society, 2015, 162(7): 311−321.

[49] SINGH K, SINGH G, SINGH H. Investigation of microstructure and mechanical properties of friction stir welded AZ61 magnesium alloy joint [J]. Journal of Magnesium and Alloys, 2018, 6(3): 292−298.

[50] WANG Qing-feng, LIU Ke, WANG Zhao-hui, LI Shu-bo, DU Wen-bo. Microstructure, texture and mechanical properties of as-extruded Mg−Zn−Er alloys containing W-phase [J]. Journal of Alloys and Compounds, 2014, 602: 32−39.

[51] HUANG Yong-xian, WANG Yao-bin, MENG Xian-chen, WAN Long, CAO Jian, ZHOU Li, FENG Ji-cai. Dynamic recrystallization and mechanical properties of friction stir processed Mg−Zn−Y−Zr alloys [J]. Journal of Materials Processing Technology, 2017, 249: 331−338.

超声辅助搅拌摩擦焊对 AZ91−C 镁合金显微组织和力学性能的影响

Faraz BARADARANI, Amir MOSTAFAPOUR, Maghsoud SHALVANDI

Faculty of Mechanical Engineering, University of Tabriz, Tabriz, Iran

摘　要：将超声辅助搅拌摩擦焊(UaFSW)与传统搅拌摩擦焊(FSW)相比，研究超声振动对 AZ91−C 镁合金显微组织和力学性能的影响。当 FSW 的转速为 1400 r/min、焊接速度为 40 mm/min 时，没有观察到缺陷。在相同条件下，引入振幅为 15 μm 超声振动，用光学显微镜和扫描电镜观察样品的显微组织。结果显示，与传统 FSW 相比，UaFSW 焊缝的显微组织更细小，原先粗大的 β-$Mg_{17}Al_{12}$ 枝晶被分离成非常细小、部分球形的颗粒，且均匀分布在 α-Mg 基体中。在超声振动和搅拌摩擦的共同作用下，材料产生严重的塑性变形，使显微组织发生明显的变化。焊缝拉伸和硬度测试的结果显示，超声振动大大提高传统 FSW 接头的力学性能，UaFSW 焊缝的抗拉强度和硬度分别从 195 MPa 和 HV 79 提高到 225 MPa 和 HV 87。

关键词：超声搅拌摩擦焊；AZ91 镁合金；显微组织；力学性能

(Edited by Bing YANG)